MINISTÉRIO DA CIÊNCIA E TECNOLOGIA
INPE
INSTITUTO DE PESQUISAS ESPACIAIS

[redacted]

1. Publication Nº	2. Version	3. Date	5. Distribution
INPE-3914-PRE/950		Jun, 1986	☐ Internal ☒ External ☐ Restricted

4. Origin: LAP — Program: PLASMA

6. Key words - selected by the author(s)
PLASMA PHYSICS ISOTOPE ENRICHMENT
ROTATING PLASMAS
PLASMA CENTRIFUGE

7. U.D.C.: 533.9

8. Title: INPE-3914-~~PRE/960~~

STEADY STATE BEHAVIOR OF ROTATING PLASMAS IN A VACUUM-ARC CENTRIFUGE

10. Nº of pages: 42

11. Last page: Fig. 9

12. Revised by

Antonio Montes

Antonio Montes

9. Authorship: J.A. Bittencourt
G.O. Ludwig

13. Authorized by

Marco Antonio Raupp
Director General

Responsible author: Bittencourt

14. Abstract/Notes

The steady state behavior of the fully ionized, multiple species, rotating, magnetized plasma in a vacuum-arc plasma centrifuge is described in detail. The analysis is based on a multiple species fluid model which includes electromagnetic, pressure gradient, centrifugal and collisional forces, for each species, in cylindrical geometry. It is shown that there is a family of theoretically possible dynamical equilibrium configurations, which can be achieved by different combinations of ion rotation velocity, radial ion density distribution and radial dependence of internal electric potential. The parametric dependences of the various plasma parameters under equilibrium conditions, including the ion separation factor, are presented for a nickel-copper plasma. The numerical results are analysed and discussed on light of experimentally measured plasma characteristics in a vacuum-arc plasma centr-fuge.

15. Remarks: To be submitted for publication in Plasma Physics and Controlled Fusion.

STEADY STATE BEHAVIOR OF ROTATING PLASMAS IN A VACUUM-ARC CENTRIFUGE

J.A. BITTENCOURT and G.O. LUDWIG
Ministério da Ciência e Tecnologia - MCT
Instituto de Pesquisas Espaciais - INPE
C.P. 515 - 12201 São José dos Campos, SP, Brasil

ABSTRACT

The steady state behavior of the fully ionized, multiple species, rotating, magnetized plasma in a vacuum-arc plasma centrifuge is described in detail. The analysis is based on a multiple species fluid model which includes electromagnetic, pressure gradient, centrifugal and collisional forces, for each species, in cylindrical geometry. It is shown that there is a family of theoretically possible dynamical equilibrium configurations, which can be achieved by different combinations of ion rotation velocity, radial ion density distribution and radial dependence of internal electric potential. The parametric dependences of the various plasma parameters under equilibrium conditions, including the ion separation factor, are presented for a nickel-copper plasma. The numerical results are analysed and discussed on light of experimentally measured plasma characteristics in a vacuum-arc plasma centrifuge.

1. INTRODUCTION

Centrifugal separation of elements and isotopes in rotating, magnetized plasma columns, has been the subject of research for many years. A comprehensive review on this subject, and the research which was done up to 1970, has been presented by Lehnert (1971). This review includes an extensive bibliography of the various investigations and surveys the theoretical considerations and experimental results for partially and fully ionized rotating, magnetized plasmas. It also summarizes the applications of rotating plasmas to nuclear fusion research, cosmical physics and technical devices such as adjustable plasma condensers, plasma guns and propulsion systems. Slepian (1955) was the first to study rotating plasmas as means for isotope enrichment. Bonnevier (1966) suggested the use of a fully ionized plasma centrifuge to enhance the mass separation effect and later studied the plasma centrifuge experimentally (Bonnevier, 1971), where a rotating fully ionized plasma was surrounded by a partially ionized plasma and neutral gas. Afterwards, several researchers have studied gas discharge plasma centrifuges and have measured isotopic enrichment in gaseous, rotating plasmas (James and Simpson, 1974, 1978; Heller and Simon, 1974; Kaneko et al., 1978; Brand et al., 1979; Wijnakker and Granneman, 1980).

A gas discharge plasma centrifuge, in its simplest configuration, consists basically of a gas at about 1 Torr pressure in a cylindrical vacuum vessel, immersed in an externally applied uniform axial magnetic field. The gas is partially ionized when current is discharged radially between two concentric cylindrical electrodes. The resulting $\underline{J} \times \underline{B}$ magnetic force density, due to radial current flow across the axial magnetic field, induces the azimuthal rotation. The centrifugal force,

acting radially outwards, causes a partial separation of the different ion species in the radial direction. The plasma centrifuge contains no moving mechanical parts, since the rotation is produced by an electromagnetic body force on the plasma and therefore can, in principle, reach much higher rotational velocities than the neutral particles in a mechanical gaseous centrifuge.

In the experiments conducted in either partially ionized or highly ionized rotating plasma columns, which were surrounded by neutral gas, the neutral atom drag on the rotating ions limits the rotational velocity to values below the Alfvēn critical velocity. Alfvēn (1960) has suggested that in a partially ionized plasma a strong enhanced ionization process arises when the directed kinetic energy of the ions, relative to the neutrals, approaches the first ionization energy of the neutrals. Additional energy input then goes selectively, via electrons, into further ionization of the neutrals, so that the ion rotational velocity is limited. Such a limiting critical velocity has been experimentally verified in rotating plasmas. Explanations for the origin of this critical velocity have been proposed by Fahleson (1961), Sockol (1968), Lehnert (1960), and McKenzie and Varma (1981). The deleterious effects of neutral atom viscous dissipation and the Alfvēn limit have resulted in relatively weak isotope enrichments in gas discharge plasma centrifuges.

More recently a new type of plasma centrifuge has been developed (Krishnan et al., 1981; Geva et al., 1981) in which the plasma source is a vacuum-arc triggered by a pulsed laser and discharged between a metallic cathode and a grounded mesh anode at one end of a 1.5m long

cylindrical vacuum vessel. Plasma rotation about the cylinder axis is sustained by the self-consistent radial electric field, produced inside the plasma column, crossed with the externally applied uniform axial magnetic field. The plasma produced in the vacuum-arc centrifuge is fully ionized and composed of the cathode material. The ionized particles evaporate from the cathode with large radial and axial velocities, and achieve rigid rotor angular rotation frequencies between 6×10^4 and 3×10^5rad/s (Krishnan et al., 1983). The absence of a neutral gas envelope and its deleterious effects has resulted in isotopic enrichments in a vacuum-arc plasma centrifuge much larger than those measured earlier in a gas discharge centrifuge. Results of element and isotope separation in various carbon and metal plasmas have been presented by Krishnan et al. (1983), and Geva et al. (1984), showing the potential for vacuum-arc plasma centrifuges to serve as practical isotope separators. They found that the centrifugal separation increases rapidly with distance from the cathode plasma source and reaches an asymptotic value at about 70cm downstream. The observations showed that the separation factor increases exponentially with the square of the radius, the electric potential profile inside the plasma has a parabolic radial dependence and the radial ion density distribution is Gaussian, in agreement with a simple, two-ion species, steady state fluid model of the rotating plasma. An improved matched impedance, low-voltage, vacuum-arc plasma centrifuge, with much better electrical efficiency than a previous prototype centrifuge, has been recently described by Prasad and Krishnan (1986).

This paper describes a three-species (electrons and two types of ions) warm fluid model used to analyse the behavior of the magnetized,

fully ionized, rotating plasma in a vacuum-arc centrifuge. Initially, in Section 2, a physical picture of the rotating plasma, based on experimental findings, is presented. The region of the arc near the cathode is still poorly understood and attention is focused on the streaming plasma region. The basic set of time-dependent multispecies fluid equations and the relevant electrodynamic equations are described in Section 3 and applied to a cylindrical column under rotation. A reduced set of time-dependent fluid equations with azimuthal symmetry is outlined, in which a Lagrangian frame of reference moving at the constant axial ion velocity is considered and the electron inertia is neglected. The resulting set of equations is further simplified considering a steady state equilibrium situation with no radial plasma motion and with the plasma column rotating as a rigid rotor. A detailed analysis of the steady state fluid equations is presented in Section 4, where a family of equilibrium solutions is identified, as there are many theoretically possible equilibrium configurations which can be achieved by different combinations of ion rotation velocity (centrifugal force), radial particle density distribution (pressure gradient force) and radial dependence of internal electric potential (electric force). Limiting equilibrium values of the various parameters and expressions for the separation factor are also discussed. A parametric numerical analysis has been carried out for the various possible equilibrium configurations of the rotating plasma column and the results are presented and discussed in Section 5. The radial distributions and parametric dependences of the various plasma variables, including the ion separation factor, are analysed on light of the experimentally observed plasma behavior in a vacuum-arc

centrifuge, considering specifically a nickel (Ni)-copper (Cu) plasma. A summary of the results and conclusions are presented in Section 6.

2. PHYSICAL PICTURE OF THE ROTATING PLASMA COLUMN

The following physical description of the rotating plasma column seems to be appropriate. The fully ionized plasma, composed of the cathode material, emanates from the cathode during the arc discharge and expands into the magnetized vacuum chamber. The electrons are effectively tied to the axial magnetic field lines, since the electron--electron collision frequency, ν_{ee}, is much smaller than the electron cyclotron frequency, Ω_{ce} ($\nu_{ee}/\Omega_{ce} \ll 1$). On the other hand, for the ions $\nu_{ii}/\Omega_{ci} \sim 0.1$ (where ν_{ii} denotes the ion-ion collision frequency and Ω_{ci} the ion cyclotron frequency), resulting in ambipolar radial diffusion in the streaming plasma region and the establishment of a self-consistent internal radial electric field $\underset{\sim}{E}_r$, which points radially inward. This radial electric field crossed with the axial magnetic induction $\underset{\sim}{B}_z$ yields an azimuthal electromagnetic plasma drift velocity

$$\underset{\sim}{u}_\theta = \underset{\sim}{E}_r \times \underset{\sim}{B}_z / B^2 \ , \tag{1}$$

which puts the plasma into rotation about the column axis. The negative radial pressure gradient crossed with the axial magnetic induction generates an azimuthal diamagnetic drift velocity

$$\underset{\sim}{u}_\theta = -(\underset{\sim}{\nabla} p)_r \times \underset{\sim}{B}_z / (n_\alpha q_\alpha B^2) \ . \tag{2}$$

Thus, this diamagnetic drift adds to the electromagnetic drift for the electrons and opposes to it for the ions, with the result that the electrons rotate faster than the ions. The resulting azimuthal current density is in the direction opposite to that of the azimuthal particle motion, so that the plasma is confined by the associated $\underset{\sim}{J}_\theta \times \underset{\sim}{B}_z$ radial force density (see Figure 1). The centrifugal force, resulting from the plasma rotation, acts radially outward and causes radial separation between particles of different mass/charge ratio. Ion-ion collisions lead to radial ion transport within the confined column, whereas ion-electron collisions lead to a relatively slow gradual diffusion of the quasi-neutral plasma across the magnetic field lines. The rotating fully ionized plasma streams axially towards the end flange and further down the column presumably reaches a quasi-steady state situation in which the net radial flux due to ion-ion collisions is zero, and the different ion species have the same angular rotation frequency. The electron angular rotation frequency, however, is still slightly higher than the ion rotation frequency, for confinement. The radial density profiles of the various species are not the same and a radial enrichment is achieved in which the heavier ion species are more abundant at large radii than lighter species.

Measurements performed by Geva et al. (1984) in a vacuum-arc fully ionized plasma centrifuge revealed the following typical values of the plasma parameters: peak (on axis) ion density $n_i \sim 10^{13} cm^{-3}$, full width at half maximum radius of a Gaussian radial density profile of 2.5cm, axial drift velocity $u_z \sim 10^6 cm/s$, mean average charge $\langle Z \rangle = 3$ for a copper/nickel plasma mixture, transit time of a plasma element across the column of 160 - 300μs, rigid rotor angular rotation

frequencies between 6×10^4 and 3×10^5rad/s, and estimated temperature of 1eV. In a more recent work, using an improved low-voltage vacuum-arc centrifuge, Prasad and Krishnan (1986) measured typical values of $n_e \sim 10^{15}cm^{-3}$ and $T_i \sim 3eV$. For typical plasma parameters of $n_e \sim 10^{13}cm^{-3}$; $<Z> = 3$, $T_e = T_i = 1eV$ and $B = 0.2T$, estimated values for various length and frequency scales of interest are as follows: Debye length $\lambda_D \sim 10^{-4}cm$, electron gyrofrequency $\Omega_{ce} \sim 10^{10}$rad/s, electron gyroradius $r_e \sim 10^{-3}cm$, ion gyrofrequency $\Omega_{ci} \sim 10^6$rad/s, ion gyroradius $r_i \sim 10^{-1}cm$, ion axial velocity $u_z \sim 10^6cm/s$, ion-ion collision frequency $\nu_{ii} \sim 10^6 - 10^7 s^{-1}$, and ion-ion collision mean free path $\lambda_{ii} \sim 0.1\text{-}1cm$. Thus, the gyroradii and collisional mean free paths are much smaller than the typical plasma column dimensions (length of about one meter and radius of a few centimeters). Also, a few rotation orbits (about five) and many collisions (of order 10^2) are experienced by a typical plasma element during its' time of transit axially down the column.

3. FLUID MODEL OF A MULTISPECIES ROTATING PLASMA

The basic set of fluid equations describing the behavior of a multispecies, rotating, magnetized warm plasma includes the equation of continuity,

$$\partial n_\alpha/\partial t + \nabla.(n_\alpha \underset{\sim}{u}_\alpha) = P_\alpha - L_\alpha \qquad (3)$$

and the momentum conservation equation, considering the effects of electromagnetic, pressure gradient and collisional forces (in the inertial laboratory frame),

$$m_\alpha\left(\frac{\partial}{\partial t} + \underset{\sim}{u}_\alpha \cdot \underset{\sim}{\nabla}\right)\underset{\sim}{u}_\alpha = Z_\alpha e(\underset{\sim}{E} + \underset{\sim}{u}_\alpha \times \underset{\sim}{B}) - \frac{1}{n_\alpha}\underset{\sim}{\nabla} p_\alpha - m_\alpha \sum_\beta \nu_{\alpha\beta}(\underset{\sim}{u}_\alpha - \underset{\sim}{u}_\beta) \ , \qquad (4)$$

where $n_\alpha(\underset{\sim}{r},t)$, $\underset{\sim}{u}_\alpha(\underset{\sim}{r},t)$ and $p_\alpha(\underset{\sim}{r},t)$ denote the number density, the fluid velocity and the partial kinetic pressure (assumed isotropic) for the type α species, respectively, P_α and L_α represent the rates of production and loss per unit volume, m_α is the particle mass, $Z_\alpha e$ is the particle charge, $\underset{\sim}{E}$ is the electric field, $\underset{\sim}{B}$ is the magnetic induction and $\nu_{\alpha\beta}$ is the collision frequency between the α and β species. Eqs. (3) and (4) must be complemented by an appropriate energy conservation equation relating $p_\alpha(\underset{\sim}{r},t)$ with $n_\alpha(\underset{\sim}{r},t)$ and $\underset{\sim}{u}_\alpha(\underset{\sim}{r},t)$. However, assuming a constant and uniform temperature T_α throughout the plasma, it is sufficient to use the ideal gas equation of state,

$$p_\alpha = n_\alpha k T_\alpha \ , \qquad (5)$$

where k denotes Boltzmann's constant.

The internal self-consistent electric field can be expressed in terms of the electric potential as $\underset{\sim}{E} = -\underset{\sim}{\nabla}\phi$, where ϕ satisfies Poisson equation inside the plasma,

$$\nabla^2\phi = -\rho/\varepsilon_0 = -(e/\varepsilon_0)\sum_\alpha Z_\alpha n_\alpha \ , \qquad (6)$$

where ρ is the total charge density. The magnetic induction produced by currents and time-dependent electric fields inside the plasma can be considered to be much smaller than the externally applied axial $\underset{\sim}{B}$ field. Therefore, Ampere's law is not considered here and the magnetic induction appearing in (4) is due only to the externally applied field.

These equations are coupled through the collisional term and through Poisson equation, and must be solved simultaneously under proper initial and boundary conditions. Eliminating $p_\alpha(\underset{\sim}{r},t)$ from (4), and considering a rotating cylindrical plasma column immersed in a constant axial magnetic induction ($\underset{\sim}{B} = B\hat{\underset{\sim}{z}}$), the following closed set of equations is obtained, in cylindrical geometry (r,θ,z),

$$\frac{\partial}{\partial t} n_\alpha + \frac{1}{r}\frac{\partial}{\partial r}(r\, n_\alpha u_{\alpha r}) + \frac{1}{r}\frac{\partial}{\partial \theta}(n_\alpha u_{\alpha\theta}) + \frac{\partial}{\partial z}(n_\alpha u_{\alpha z}) = 0 \ , \tag{7}$$

$$m_\alpha\left(\frac{D}{Dt} u_{\alpha r} - \frac{u_{\alpha\theta}^2}{r}\right) = Z_\alpha e(E_r + u_{\alpha\theta}B) - kT_\alpha \frac{\partial}{\partial r} \ell n(n_\alpha) - m_\alpha \sum_\beta \nu_{\alpha\beta}(u_{\alpha r} - u_{\beta r}) \ , \tag{8}$$

$$m_\alpha\left(\frac{D}{Dt} u_{\alpha\theta} + \frac{u_{\alpha\theta}u_{\alpha r}}{r}\right) = Z_\alpha e(E_\theta - u_{\alpha r}B) - kT_\alpha \frac{1}{r}\frac{\partial}{\partial \theta} \ell n(n_\alpha) - m_\alpha \sum_\beta \nu_{\alpha\beta}(u_{\alpha\theta} - u_{\beta\theta}), \tag{9}$$

$$m_\alpha \frac{D}{Dt} u_z = Z_\alpha e E_z - kT_\alpha \frac{\partial}{\partial z} \ell n(n_\alpha) - m_\alpha \sum_\beta \nu_{\alpha\beta}(u_{\alpha z} - u_{\beta z}) \ , \tag{10}$$

$$\frac{1}{r}\frac{\partial}{\partial r}\left(r \frac{\partial \phi}{\partial r}\right) + \frac{1}{r^2}\frac{\partial^2 \phi}{\partial \theta^2} + \frac{\partial^2 \phi}{\partial z^2} = -\frac{e}{\varepsilon_0} \sum_\alpha Z_\alpha n_\alpha \ , \tag{11}$$

where the production and loss terms have been neglected and D/Dt denotes the substantial or total time derivative

$$\frac{D}{Dt} = \frac{\partial}{\partial t} + u_{\alpha r}\frac{\partial}{\partial r} + \frac{1}{r} u_{\alpha\theta}\frac{\partial}{\partial \theta} + u_{\alpha z}\frac{\partial}{\partial z} \ . \tag{12}$$

If the number of different species considered is denoted by a, then (4a + 1) coupled scalar equations will have to be solved simultaneously in order to determine the variables n_α, $u_{\alpha r}$, $u_{\alpha\theta}$, $u_{\alpha z}$ and ϕ.

When the plasma density is relatively high and/or the internal electric potential relatively small, it becomes inconvenient to look for a numerical solution of Poisson equation, since the total charge density ρ required to produce the potential ϕ becomes an extremely small fraction of the electron (or ion) charge density $Z_\alpha e n_\alpha$. This situation holds in the bulk part of the rotating high-density plasma in the vacuum-arc centrifuge, where $n_e \sim 10^{13} cm^{-3}$ (Geva et al., 1984), although it may not be applicable in the plasma sheath region near the boundaries of the rotating plasma column. Thus, in the bulk part of the plasma, instead of solving Poisson equation numerically, it is appropriate to consider the plasma quasi-neutrality approximation

$$\sum_\alpha Z_\alpha n_\alpha = 0 \ , \tag{13}$$

even though there is an internal electric field.

In order to proceed further, some simplifying assumptions will be made. The rotating plasma column is assumed to be azimuthally symmetric, so that all variables are independent of θ. Thus, all θ-derivatives vanish and $E_\theta = 0$. Further, considering time scales appropriate to analyse the ion motion, electron inertia can be neglected. Thus, from (9) it is seen that $u_{er} = 0$. The electrons are therefore tightly coupled to the axial magnetic field lines. For regions not too close to the source of plasma particles (cathode), it is experimentally justified (Geva et al., 1984) to consider the axial velocity $u_{\alpha z}$ to be constant. In this case $Du_{\alpha z}/Dt = 0$. If a longitudinal current flows in the plasma, then $u_{ez} \neq u_{iz}$, although u_{iz} can be considered to be the same for the different ion species. Geva et al. (1984) observed a constant ion

axial drift velocity $u_{iz} \sim 10^6$cm/s, independent of radial and axial location inside the plasma column, with slightly different values for different types of plasmas.

Furthermore, it is convenient to consider a Lagrangian reference frame moving at the constant axial ion velocity u_{iz}. Thus, a substantial time derivative is defined according to

$$\frac{d}{dt} = \frac{\partial}{\partial t} + u_{iz} \frac{\partial}{\partial z} \, . \tag{14}$$

In this axially moving reference frame all ion motions occur in the (r,θ) plane and, consequently, all ion variables become explicit functions of only r and t. The z-dependence is intrinsically incorporated in the time-dependence seen in the moving frame and the boundary conditions specified at $z = z_0$ can be viewed as initial conditions at $t = t_0$. Geva et al. (1984) found that the axial electric field is of the order of 1V/m, much smaller than the radial field (of order 10^3V/m), so that the number densities depend much more strongly on r than on z.

With these assumptions, the set of equations (7)-(10) can be written (with $u_{er} = 0$) as

$$\left(\frac{d}{dt} - \frac{J_z}{en_e} \frac{\partial}{\partial z}\right) n_e = 0 \, , \tag{15}$$

$$\frac{d}{dt} n_i + \frac{1}{r} \frac{\partial}{\partial r}(r n_i u_{ir}) = 0 \, , \tag{16}$$

$$-e(E_r + u_{e\theta} B) - kT_e \frac{\partial}{\partial r} \ell n(n_e) = 0 \, , \tag{17}$$

$$\frac{d}{dt} u_{ir} + u_{ir} \frac{\partial}{\partial r} u_{ir} - \frac{u_{i\theta}^2}{r} = \frac{Z_i e}{m_i} (E_r + u_{i\theta} B) -$$

$$- \frac{kT_i}{m_i} \frac{\partial}{\partial r} \ell n (n_i) - \sum_j \nu_{ij} (u_{ir} - u_{jr}) , \qquad (18)$$

$$\frac{d}{dt} u_{i\theta} + u_{ir} \frac{\partial}{\partial r} u_{i\theta} + \frac{u_{i\theta} u_{ir}}{r} = \frac{Z_i e}{m_i} u_{ir} B - \sum_j \nu_{ij} (u_{i\theta} - u_{j\theta}) , \qquad (19)$$

$$Z_\alpha e E_z - kT_\alpha \frac{\partial}{\partial z} \ell n (n_\alpha) = 0 \qquad (\alpha = e,i) , \qquad (20)$$

where the index α denotes electrons or ions, e denotes electrons and i the ion species, and $J_z = -en_e(u_{ez} - u_{iz})$. If J_z vanishes, then (15) yields a constant electron number density in the axially moving frame ($dn_e/dt = 0$). Eq. (20) is decoupled from (17)-(19) and shows that the electron and ion number densities vary longitudinally according to the Boltzmann factor,

$$n_\alpha(r,z,t) = n_\alpha(r,z_0,t) \exp \left\{ - \frac{Z_\alpha e}{kT_\alpha} [\phi(r,z,t) - \phi(r,z_0,t)] \right\} . \qquad (21)$$

The original set of coupled non-linear partial differential equations (7)-(11) has now been reduced to a closed set involving the variables n_α, u_{ir}, $u_{\alpha\theta}$ and ϕ, with r and t as independent variables.

From the experimentally observed axial evolution of the separation factor and plasma density radial profiles, it is seen that the plasma achieves a quasi-equilibrium at about 70cm downstream from the cathode, with a transit time which varies between 160μs to 300μs (Geva et al., 1984).

In this quasi-equilibrium region the changes with respect to z are much smaller than over comparable intervals in the region close to the cathode, and the radial velocity components are much smaller than the other ones, so that the plasma essentially rotates in the θ-direction in the axially moving frame. The different ion species are expected to achieve the same rotational velocity at each radial position ($u_{i\theta} = u_{j\theta}$), as a result of ion-ion collisions. The electrons, of course, may have a higher rotational velocity than the ions, due to their negligible inertia, thus providing a confining $\underset{\sim}{J}_\theta \times \underset{\sim}{B}$ radial force density. Also, it has been shown experimentally that the plasma rotates as a rigid body in its bulk part (except, perhaps, in the sheath region), so that $u_{\alpha\theta} = \omega_\alpha r$, where ω_α is the angular rotation frequency.

In what follows it is considered an isothermal, multispecies, magnetized plasma column rotating as a rigid body under steady state conditions, with no axial dependence (infinitely long column), and with no boundary conditions involved. Thus, the plasma is uncoupled from the cathode, the anode mesh and the walls, so that their effects are not considered. In this case, (16) yields $u_{ir} = 0$, since there is no spatial plasma source to allow for a non-vanishing radial plasma flux. Eq. (19) gives no information, since $u_{ir} = 0$, whereas (18) becomes

$$m_i \omega_i^2 r + Z_i e(E_r + \omega_i r B) - kT_i \frac{\partial}{\partial r} \ln(n_i) = 0 \ . \qquad (22)$$

4. ANALYSIS OF STEADY STATE FLUID EQUATIONS

A family of equilibrium solutions is obtained from (17) and (22), together with the plasma neutrality approximation (13). A parametric numerical analysis can be made, for example, ω_i and $E_r(r)$ can be

specified and (22) used to determine $n_i(r)$, for $i = 1,2$. The plasma neutrality approximation then yields $n_e(r)$, which allows the calculation of ω_e from (17). From (17) and (22) explicit expressions for $n_e(r)$ and $n_i(r)$ can be derived in terms of the other variables as

$$n_e(r) = n_e(0) \exp\left[- \frac{e}{kT_e} \int_0^r E_r dr - \frac{e\omega_e B r^2}{2kT_e} \right] , \tag{23}$$

$$n_i(r) = n_i(0) \exp\left[\frac{Z_i e}{kT_i} \int_0^r E_r dr + \frac{m_i \omega_i}{2kT_i} (\omega_i + \Omega_i) r^2 \right] , \tag{24}$$

where $\Omega_i = Z_i eB/m_i$ denotes the ion cyclotron frequency.

Useful information can be further obtained from (17) and (22) by solving them explicitly for the angular rotational frequencies. From (17) it is obtained, for the electrons,

$$\omega_e = \frac{1}{r} \left[- \frac{E_r}{B} - \frac{kT_e}{eB} \frac{\partial}{\partial r} \ell n(n_e) \right] , \tag{25}$$

showing that ω_e is due to the electromagnetic plus the diamagnetic drift velocities. Note that these drift velocities are both in the positive θ-direction for $\underset{\sim}{E}$ and $\underset{\sim}{\nabla} p$ pointing radially inwards. Furthermore, for a rigid rotor ω_e must be independent of r, so that if E_r is proportional to r then $\ell n(n_e)$ must be proportional to r^2, in agreement with the experimental observations of Geva et al. (1984). Therefore,

$$\underset{\sim}{E}_r(r) = E_r \hat{\underset{\sim}{r}} = -ar\hat{\underset{\sim}{r}} \qquad (a > 0) , \tag{26}$$

$$\phi(r) - \phi(0) = ar^2/2 , \tag{27}$$

$$n_e(r) = n_e(0)\ \exp(-\beta_e r^2)\ , \tag{28}$$

where a and β_e are constants, so that E_r varies linearly with radius, $\phi(r)$ shows a parabolic radial dependence and $n_e(r)$ has a Gaussian radial distribution across the column, with β_e given by

$$\beta_e = \frac{e}{2kT_e}\ (\omega_e B - a)\ . \tag{29}$$

Note that, since $a > 0$, the condition $\omega_e > a/B$, or equivalently, $u_{e0} > -E_r/B$, must be satisfied for confinement. Otherwise, $\partial n_e/\partial_r \geq 0$. Thus, the electron rotation must be larger than the electromagnetic drift rotation velocity.

Eq. (22) can be solved explicitly for the ion rotation frequency, yielding

$$\omega_i = \frac{1}{2}\ \Omega_{ci}\left\{-1 \pm \left[1 - \frac{4E_r/B}{\Omega_{ci} r} + \frac{4kT_i}{m_i \Omega_{ci}^2 r}\ \frac{\partial}{\partial r}\ \ell n\ (n_i)\right]^{1/2}\right\}\ . \tag{30}$$

This result also shows that for rigid body rotation (constant ω_i) E_r can be chosen proportional to r and $\ell n(n_i)$ proportional to r^2, according to the experimental observations of Geva et al. (1984). Thus $n_i(r)$ also has a Gaussian radial distribution

$$n_i(r) = n_i(0) \exp(-\beta_i r^2) \tag{32}$$

with the constant β_i given by

$$\beta_i = \frac{Z_i e}{2kT_i}\left[a - \omega_i B\left(1 + \frac{\omega_i}{\Omega_{ci}}\right)\right] . \qquad (32)$$

For confinement ($\partial n_i/\partial r < 0$), the condition $\beta_i > 0$ must hold, which corresponds to

$$u_{i\theta} < - \frac{E_r/B}{(1 + \omega_i/\Omega_{ci})} . \qquad (33)$$

Thus, the ions rotate at a velocity which is smaller than the electromagnetic drift velocity, for confinement. It should be also noted, from (30), that the diamagnetic drift velocity for the ions is opposite to the electromagnetic drift velocity, considering $\underset{\sim}{E}$ and $\underset{\sim}{\nabla}p$ pointing radially inwards. This differential rotation velocity between electrons and ions provides the $\underset{\sim}{J}_\theta \times \underset{\sim}{B}$ confining radial force density.

Eq. (30) also shows the existence of two families of solutions for ω_i, having ω_i either positive or negative. Experimentally it is observed that the ions rotate in the positive θ-direction, for $\underset{\sim}{B}$ pointing along $\hat{\underset{\sim}{z}}$. This is expected on physical grounds because as soon as the plasma is generated at the cathode and expands into the magnetized vacuum chamber, the electrons tend to remain tied to the magnetic field lines (since $\nu_{ee}/\Omega_{ce} << 1$), so that their transverse motion is inhibited due to the negligibly small electron inertia, whereas the ions tend to diffuse across the field lines, thus generating a transverse polarization electric field, due to charge separation, which points radially inward. This electric field, crossed with the axial magnetic field, induces the plasma rotation in the positive θ-direction. It must be noted that the solutions with negative ω_i imply in a strongly diamagnetic equilibrium,

with a large azimuthal current density and greatly compressed plasma column. When the diamagnetic drift exceeds the $\underline{E} \times \underline{B}$ drift, the ions rotate in the negative θ-direction, whereas the electrons rotate at more than twice the $\underline{E} \times \underline{B}$ drift velocity in the positive θ-direction. Thus, the family of solutions with negative ω_i will not be considered here, since it is not relevant to the experimentally observed plasma behavior in a vacuum-arc centrifuge.

The family of solutions with the plus sign in (30) also has a branch in which ω_i is still negative. Eq. (30), with the plus sign, can be rewritten as

$$\omega_i = \frac{1}{2}\Omega_{ci}\left(-1 + D^{1/2}\right) , \tag{34}$$

where D denotes the discriminant

$$D = 1 - \frac{4E_r/B}{\Omega_{ci} r} + \frac{4kT_i}{m_i \Omega_{ci}^2 r} \frac{\partial}{\partial r} \ln (n_i) . \tag{35}$$

Real solutions require $D \geq 0$, whereas for positive ω_i it is required $D \geq 1$. Therefore, for positive ω_i, the following condition is obtained from (35)

$$n_i(r) \geq n_i(0) \exp\left\{ - \frac{Z_i e}{kT_i} \left[\phi(r) - \phi(0) \right] \right\} . \tag{36}$$

The equal sign corresponds to the limit of no-rotation, so that this result can also be obtained from (22) taking $u_{ir}=0$. Eq. (36) shows that for each electric potential radial curve there corresponds a

minimum Gaussian density radial distribution which gives the no-rotation limit. The parametric curves for all positive values of ω_i must yield Gaussian radial density distributions which lie above this lower limiting Gaussian curve. Furthermore, for confined plasmas ($\beta_i > 0$), the upper limit given in (33) for ω_i must be observed. The value of ω_i corresponding to $\beta_i = 0$ (uniform plasma with vanishing radial pressure gradient) can be obtained from (30) or (33) as

$$\omega_i = \frac{1}{2}\Omega_{ci}\left[-1+\left(1-\frac{4E_r/B}{\Omega_{ci}r}\right)^{1/2}\right] . \tag{37}$$

If $|E_r|/B \ll \Omega_{ci}r/4$, then the square root term in (37) can be expanded in a Taylor series with the result that, to lowest order, the upper limit of ω_i is given by the $\underline{E} \times \underline{B}$ angular rotation velocity ($\omega_i = a/B$).

For purposes of element or isotope separation analysis, it is appropriate to define a separation factor $\alpha_0(r)$ between any two ion species as

$$\alpha_0 = \frac{n_i(r)/n_j(r)}{n_i(0)/n_j(0)} . \tag{38}$$

For a rigid rotor equilibrium with the ion densities given by (24), the separation factor becomes

$$\alpha_0(r) = \exp\left\{\frac{r^2}{2k}\left[e\left(\frac{Z_i}{T_i}-\frac{Z_j}{T_j}\right)(\omega B - a)+\omega^2\left(\frac{m_i}{T_i}-\frac{m_j}{T_j}\right)\right]\right\} , \tag{39}$$

where $\omega = \omega_i = \omega_j$. If both ions have the same temperature ($T_i = T_j$) and the same charge ($Z_i = Z_j$), then (39) reduces to the usual expression for

the separation factor of a gaseous centrifuge. In general, a modified separation factor $\alpha(r)$ can be defined as

$$\alpha(r) = \frac{[n_i(r)]^{1/Z_i}/[n_j(r)]^{1/Z_j}}{[n_i(0)]^{1/Z_i}/[n_j(0)]^{1/Z_j}} = \exp\left[\left(\frac{m_i}{Z_i} - \frac{m_j}{Z_j}\right)\frac{\omega^2 r^2}{2kT}\right] . \qquad (40)$$

In this way, the radial potential difference across the column is conveniently eliminated.

As a final remark in this analysis, it is to be noted that an approximation is involved when using the rigid rotor assumption together with the plasma neutrality condition. This approximation is reasonable as long as the Gaussian density radial distributions for the ions do not differ significantly from one another, so that their sum is still approximately Guassian.

5. RESULTS AND DISCUSSION

A parametric analysis is carried out for the steady state equilibrium of a multispecies, fully ionized, rotating plasma composed of ions of Ni and Cu, whose atomic weights are 58.70 and 63.55, respectively. The numerical results presented and discussed in this section are for a 50% Ni and 50% Cu plasma mixture, although any other type of fully ionized plasma could have been considered, including an isotopic mixture of the same element for purposes of isotope separation analysis. Results are presented for singly ionized and for triply ionized ions, since Geva et al. (1984) found a mean charge $\langle Z \rangle = 3$ for both Ni and Cu. Various strengths of the magnetic field are considered in order to investigate the effect of the magnetic field on the plasma parameters and separation factor. Values used for the particle number densities

at the column axis are $n_1 = n_2 = 10^{13}cm^{-3}$ and $n_e = 2 \times 10^{13}cm^{-3}$ (for singly ionized ions) or $n_e = 6 \times 10^{13}cm^{-3}$ (for triply ionized ions), which are typical experimental values according to Geva et al. (1984). The electron and ion temperatures are assumed to be the same and equal to 10^4K. The limiting radial distance is taken as $R_0 = 10cm$ and the electric potential differences are specified between the column axis ($r = 0$) and R_o, i.e, $\Delta\phi = \phi(0) - \phi(R_o)$, where $\phi(r)$ has a parabolic dependence according to (27). Thus, $\Delta\phi$ is always negative.

A family of equilibrium solutions, obtained from (22), (17) and (13), is presented in Figure 2, showing the radial distribution of the heaviest ion (Cu) number density for various values of ω_i (in units of 10^4Hz) as parameter and for various values of $\Delta\phi$, considering $B = 0.2T$ and $Z_i = 1$. Important points to be noted in this figure are: (a) the full width at half maximum (FWHM) normalized radius of the Gaussian density radial distribution, in the no-rotation limit ($\omega_i = 0$), decreases with increasing $\Delta\phi$; (b) ω_i increases with $\Delta\phi$ and with the FWHM; (c) the permissible range of values of ω_i considering a FWHM normalized radius between 0.2 and 0.3, say, for each value of $\Delta\phi$, decreases sharply with increasing $\Delta\phi$. Although $\Delta\phi$ has been specified between $r = 0$ and $r = R_0 = 10cm$, for purposes of comparison with experimental results, the electric potential difference to be considered should be taken between the column axis ($r = 0$) and the radial distance in which the plasma density is still significant, i.e. just before the plasma sheath region.

The radial number density distribution of the lightest ion (Ni) is not shown here. However, the radial dependence of the separation factor, defined according to (38), is presented in Figure 3, with ω_i

in units of 10^4Hz) as parameter. It must be noted that $\omega_0(r)$ increases sharply with ω_i and r. The sum of the values of $n_i(r)$ (for i = 1,2), at each radial position, gives $n_e(r)$, according to (13).

It is of interest to compare the ion angular rotation frequencies presented in Figure 2 with the corresponding ion cyclotron frequencies $Z_i eB/m_i$, and electromagnetic $\underline{E} \times \underline{B}$ angular rotation frequencies, $|E_r|/rB$. For most cases ω_i is usually less than Ω_{ci}, but it may exceed Ω_{ci} for sufficiently large values of $\Delta\phi$, since ω_i increases with $\Delta\phi$ for a given B field and FWHM. On the other hand, for a confined plasma ($\partial n_i/\partial r < 0$), ω_i is always smaller than $|E_r|/rB$, as discussed previously. For $\omega_i = |E_r|/rB$ the radial ion pressure gradient is positive. However, for values of the FWHM normalized radius greater than, say, 0.2 and for relatively large values of $\Delta\phi$, the effect of the diamagnetic drift becomes small, so that ω_i may get very close to the electromagnetic drift ($\omega_i \lesssim |E_r|/rB$).

The results shown in Figure 2 can be presented in a more compact manner without explicitly showing the radial dependence of $n_i(r)$. The variables involved are ω_i, $\Delta\phi$ and the FWHM for $n_z(r)$, where the radial dependences are linear for $u_i(r)$, parabolic for $\phi(r)$ and Gaussian for $n_i(r)$. Thus, Figure 4 shows ω_i versus $\Delta\phi$, with the FWHM normalized radius as parameter, corresponding to the results presented in Figure 2. The most important feature is the sharp decrease in the range of allowed equilibrium values of ω_i, as $\Delta\phi$ increases, considering a given range of values for the FWHM. The arrows along the abscissa indicate the corresponding asymptotic value for each parametric curve. Thus, fixing one value of the FWHM, its corresponding parametric curve indicates how ω_i and $\Delta\phi$ must vary according to equilibrium conditions. Alternatively, choosing any reasonable values for two of these parameters, the other one is uniquely determined.

Another variable which is uniquely determined once any two of the parameters ω_i, $\Delta\phi$ and FWHM are kept fixed, is ω_e, as can be seen from (17), since $n_e(r)$ is determined by charge neutrality. For illustration purposes, it is presented in Figure 5 the FWHM normalized radius for $n_2(r)$ (full lines) and ω_e (dashed lines) as a function of $\Delta\phi$, in the limit of no ion rotation ($\omega_i = 0$), for several values of B and Z_i as parameters. Note that the lines for the FWHM are independent of B. It is seen that the FWHM decreases with $\Delta\phi$, whereas ω_e increases with $\Delta\phi$, but decreases with B. Also, the FWHM decreases as ω_e increases, since for $\omega_i = 0$ the radial confining force on the plasma is due to the azimuthal electron current.

Four principal variables are therefore involved in order to picture the steady state behavior of the rotating plasma column, which are ω_i, ω_e, $\Delta\phi$ and the FWHM for $n_2(r)$. The relationship between these four variables under equilibrium conditions is illustrated in Figure 6, where it is shown ω_i as a function of ω_e, with both $\Delta\phi$ and the FWHM normalized radius as parameters, for $B = 0.2T$ and $Z_i = 3$. The arrows along the abscissa indicate the asymptotic values corresponding to each parametric curve for $\Delta\phi$. The dashed straight line is the 45^o slope line, for which $\omega_i = \omega_e$. The dashed curve in the region where $\omega_i > \omega_e$ indicates the situation in which $\omega_i = |E_r|/rB$. Note that, since $m_2 > m_1$ (where the indices 1 and 2 denote Ni and Cu, respectively), when the conditions are such that the FWHM for n_2 tends to infinity (constant density for Cu), $n_1(r)$ still shows a negative radial gradient. For a higher value of ω_i such that n_1 becomes radially uniform, $n_2(r)$ will already show a positive radial gradient. The allowed values of the various variables for a confined plasma are located in the region where $\omega_e > \omega_i$.

Experimentally observed values of the FWHM normalized radius are around 0.25 (Geva et al., 1984), so that the FWHM parametric curves labeled 0.2 and 0.3 presumably limits the region where the experimentally observed points should be located, under equilibrium conditions. For relatively large values of $\Delta\phi$ this region becomes extremely small. Comparing with Figure 2, it is seen that the increase in the value of Z_i reduces the FWHM in the limit of no-rotation and increases slightly the ω_i values, for a given $\Delta\phi$, the effect being more pronounced for large values of $\Delta\phi$. For example, considering $\Delta\phi = -100V$ and a FWHM normalized radius of 0.25, Figure 2 yields $\omega_i = 7 \times 10^4$rad/s, whereas Figure 6 yields $\omega_i = 9 \times 10^4$rad/s. In both cases $\omega_e \geq 10^5$rad/s.

A plot similar to the one in Figure 6 is shown in Figure 7 for the case in which $B = 1.0T$ and $Z_i = 3$, in order to show the dependence of the various equilibrium variables on the magnetic field. It is seen that smaller ω_i values are obtained as B increases, for the same values of $\Delta\phi$ and FWHM. For example, considering $\Delta\phi = -100V$ and a FWHM normalized radius of 0.25, it is obtained $\omega_i = 2 \times 10^4$rad/s from Figure 7. Comparing Figures 6 and 7, it is seen that the FWHM in the no-rotation limit does not change with B, as it depends only on the pressure gradient and the radial dependence of $\phi(r)$. It should be noted that the sharp decrease in ω_i as B increases, seen when comparing Figures 6 and 7, does not necessarily mean, in a practical situation, that ω_i decreases as B is increased, since experimentally (Geva et al., 1984) it is observed that $\Delta\phi$ varies with B and it depends also on other parameters such as the geometry and nature of the produced plasma. Therefore, the dependence of $\Delta\phi$ on B should be determined experimentally for each type of plasma being analysed,

in order to select the B value which maximizes ω_i.

Measurements made by Geva et al. (1984) for a Ni-Cu plasma, at about 90cm downstream from the cathode, showed a Gaussian radial ion density distribution with a FWHM radius of 2.5cm, a parabolic radial dependence for $\phi(r)$ inside the plasma with a potential drop of about 8V between $r = 0$ and $r = 3$cm (which extrapolates to $\Delta\phi = 89$V at $r = 10$cm), and $\omega_i = 7.9 \times 10$ rad/s, for $B = 0.13$T and $\langle Z_i \rangle = 3$ (Figure 11 of Geva et al., 1984). These experimental results are in good agreement with the theoretical predictions for steady state equilibrium conditions, presented in Figure 6, considering the uncertainties and approximations involved.

Figure 8 illustrates explicitly the dependence of ω_i on B for several values of $\Delta\phi$, considering $Z_i = 3$. The parametric curves indicate the corresponding values of the FWHM normalized radius and the number within parenthesis refers to the limiting value of the FWHM when ω_i goes to zero. Note that the region limited by the lines corresponding to a FWHM normalized radius between 0.2 and 0.3, say, decreases sharply as $\Delta\phi$ increases and tends to just one single line for sufficiently large values of $\Delta\phi$. Hence, in this case, ω_i is uniquely determined for specified values of $\Delta\phi$ and B. It must be stressed that this inverse dependence of ω_i with B is valid for a constant value of $\Delta\phi$. However, as mentioned before, the experimentally observed values of $\Delta\phi$ depend on B as well as on other plasma characteristics, so that the dependence of ω_i on B in a practical situation is not that straigth-forward. For each experimental situation a relationship between $\Delta\phi$ and B must be determined first, in order to find how ω_i varies with B (and $\Delta\phi$). This is an important aspect to be investigated in order to

derive scaling laws for plasma centrifuges, since there must be a certain value of B, for a given plasma, which maximizes ω_i and therefore the separation factor.

Finally, for the purpose of element and isotope separation analysis, once the ion rotation frequency has been determined, it is shown in Figure 9 the dependence of α_0 on the mass difference Δm (in atomic mass units) between any two ion species, with ω_i (in units of 10^6 Hz) as parameter, at a normalized radial distance $r/R_0 = 0.5$. The importance of achieving large values of ω_i is clearly evident from this plot, if large values of α_0 are to be obtained.

6. SUMMARY AND CONCLUSIONS

A multiple species fluid model for a fully ionized, magnetized plasma under rotation has been described, which includes electromagnetic, pressure gradient, centrifugal and collisional forces, in cylindrical geometry. A detailed numerical analysis is presented for the steady state behavior of a fully ionized rotating plasma column in a vacuum-arc centrifuge and the parametric dependence of the various plasma variables is established considering a Ni-Cu plasma. A family of theoretically possible equilibrium configurations is obtained for various combinations of centrifugal, pressure gradient and electromagnetic forces. It is shown that the ion rotation frequency, and therefore the separation factor, increase with the radial electric potential difference (for a given magnetic induction), but decrease as the magnetic induction increases (for a given radial electric potential difference). The theoretical results show that, essentially,

the electron angular rotation frequency is larger than, and the ion angular rotation frequency smaller than the $\underset{\sim}{E} \times \underset{\sim}{B}$ angular rotation frequency, the difference being dependent on the FWHM radius of the Gaussian radial density distribution. Since the ion rotation frequency approaches the upper limiting velocity for confinement (which is slightly less than the $\underset{\sim}{E} \times \underset{\sim}{B}$ drift velocity) as the inward radial pressure gradient decreases, it seems convenient to produce a plasma column with a small radial pressure gradient and therefore with a large FWHM radius, in order to achieve higher rotational velocities. This situation also gives a larger plasma density at the outer radii than otherwise, thus increasing the quantity of enriched plasma. Also, experimental observations have shown that $\Delta\phi$ and B_z depend on one another, and this relationship depends further on the plasma characteristics and geometry. Therefore, it is important to experimentally determine the relationship between $\Delta\phi$ and B_z, for each situation under investigation in a vacuum-arc centrifuge, with a view to establishing scaling laws for such centrifuges. An appropriate value of B_z can then be selected in order to maximize the ion rotation velocity and the separation factor. The FWHM radius of the ion density radial distribution is another factor which affects the ion rotation velocity and it seems that the cathode geometry, the divergence of the magnetic field lines near the cathode target and the distance of the anode mesh to the target may play an important role in determining the column radial dimensions. Further experiments and analysis are therefore suggested in order to optimize the vacuum-arc centrifuge parameters and for development of such devices into practical isotope separators.

The results of the steady state analysis presented here are in good agreement with experimental findings for the plasma behavior in a vacuum-arc centrifuge, as the plasma column reaches an asymptotic, quasi-steady behavior at about 70cm downstream from the cathode. A time-dependent analysis can shed some light on how this quasi-equilibrium in attained within a few ion rotation orbits about the column axis.

REFERENCES

ALFVEN, H. (1960) Rev. Mod. Phys. 32, 710.

BONNEVIER, B. (1971) Plasma Phys. 13, 763.

BONNEVIER, B. (1966) Arkiv Fysik 33, 255

BRAND, G.F.; JAMES, B.W. and WALSH, C.J. (1979) J. Phys. D 12, 1495.

FAHLESON, U.V. (1961) Phys. Fluids 4, 123.

GEVA, M.; KRISHNAN, M. and HIRSHFIELD, J.L. (1984) J. Appl. Phys. 56, 1398.

GEVA, M.; KRISHNAN, M. and HIRSFIELD, J.L (1981) Nucl.Instrum.Meth. 186, 183.

HELLER, H. and SIMON, M. (1974) Phys. Lett. 50A, 139.

JAMES, B.W. and SIMPSON, S.W. (1978) Plasma Phys. 20, 759.

JAMES, B.W. and SIMPSON, S.W. (1974) Phys. Lett. 46A, 347.

KANEKO, O.; SASAKI, S. and KAWASHIMA, M. (1978) Plasma Phys. 20, 1167.

KRISHNAN, M.; GEVA, M. and HIRSHFIELD, J.L. (1983) Phys. Fluids 26, 2676.

KRISHNAN, M.; GEVA, M. and HIRSHFIELD, J.L. (1981) Phys. Rev. Lett. 46, 1.

LEHNERT, B. (1971) Nucl. Fusion 11, 485.

LEHNERT, B (1960) Rev. Mod. Phys. 32, 1012.

MCKENZIE, J.F. and VARMA, R.K. (1981) J. Plasma Phys. 25, 491.

PRASAD, R.R. and KRISHNAN, M. (1986) Rev. Sci. Instrum. 57, 74.

SLEPIAN, J. (1955) J. Appl. Phys. 26, 1283.

SOCKOL, P.M. (1968) Phys. Fluids 11, 637.

WIJNAKKER, M.M.B. and GRANNEMAN, E.H.A. (1980) Z. Naturforsch 35A, 883.

FIGURE CAPTIONS

Fig. 1 - Schematic representation of the rotating plasma in the (r,θ) plane showing the relative orientations of the electric and magnetic fields, the particle azimuthal rotation velocities and the azimuthal current density.

Fig. 2 - Radial number density distribution of the heaviest ion (Cu) for various values of the electric potential difference $\Delta\phi$ between the column axis and the $R_0 = 10$cm radial distance, with the ion rotation frequency ω_i(in units of 10^5Hz) as parameter, for $B = 0.2$T and $Z_i = 1$.

Fig. 3 - Radial dependence of the separation factor α_0 for the Ni-Cu plasma mixture (for which $\Delta m = 4.85$amu), with the ion rotation frequency ω_i (in units of 10^5Hz) as parameter.

Fig. 4 - Ion rotation frequency ω_i as a function of the electric potential difference $\Delta\phi$ between the column axis and the $R_0 = 10$cm radial distance, with the full width at half maximum (FWHM) normalized radius r/R_0 as parameter, for $B = 0.2$T and $Z_i = 1$.

Fig. 5 - Full width at half maximum (FWHM) normalized radius r/R_0 (full lines) and electron rotation frequency ω_e (dashed lines) as a function of the electric potential difference $\Delta\phi$ between the column axis and the $R_0 = 10$cm radial distance, in the limit of no ion rotation ($\omega_i = 0$), with the magnetic induction B and the ionization state Z_i as parameters.

Fig. 6 - Ion rotation frequency ω_i as a function of the electron rotation frequency ω_e, having as parameters the full width at half maximum (FWHM) normalized radius r/R_0 and the electric potential difference $\Delta\phi$ between the column axis and the $R_0 = 10cm$ radial distance, for $B = 0.2T$ and $Z_i = 3$.

Fig. 7 - Same as in Fig. 6, but for $B = 1.0T$ and $Z_i = 3$.

Fig. 8 - Dependence of the ion rotation frequency ω_i on the magnetic induction B, with the full width at half maximum (FWHM) normalized radius r/R_0 as parameter, for various values of the electric potential difference $\Delta\phi$ between the column axis and the $R_0 = 10cm$ radial distance.

Fig. 9 - Dependence of the separation factor α_0 on the mass difference Δm (in amu) between any two ion species considered, at the radial distance $r/R_0 = 0.5$, with the ion rotation frequency ω_i (in units of $10^4 Hz$) as parameter.

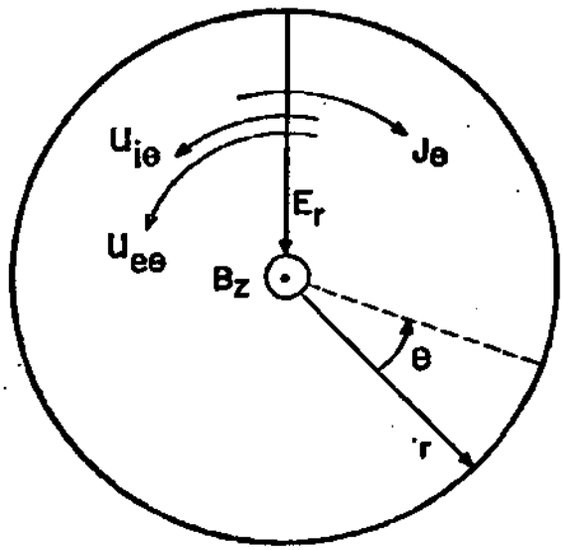

Fig. 1 - J.A. Bittencourt and G.O. Ludwig

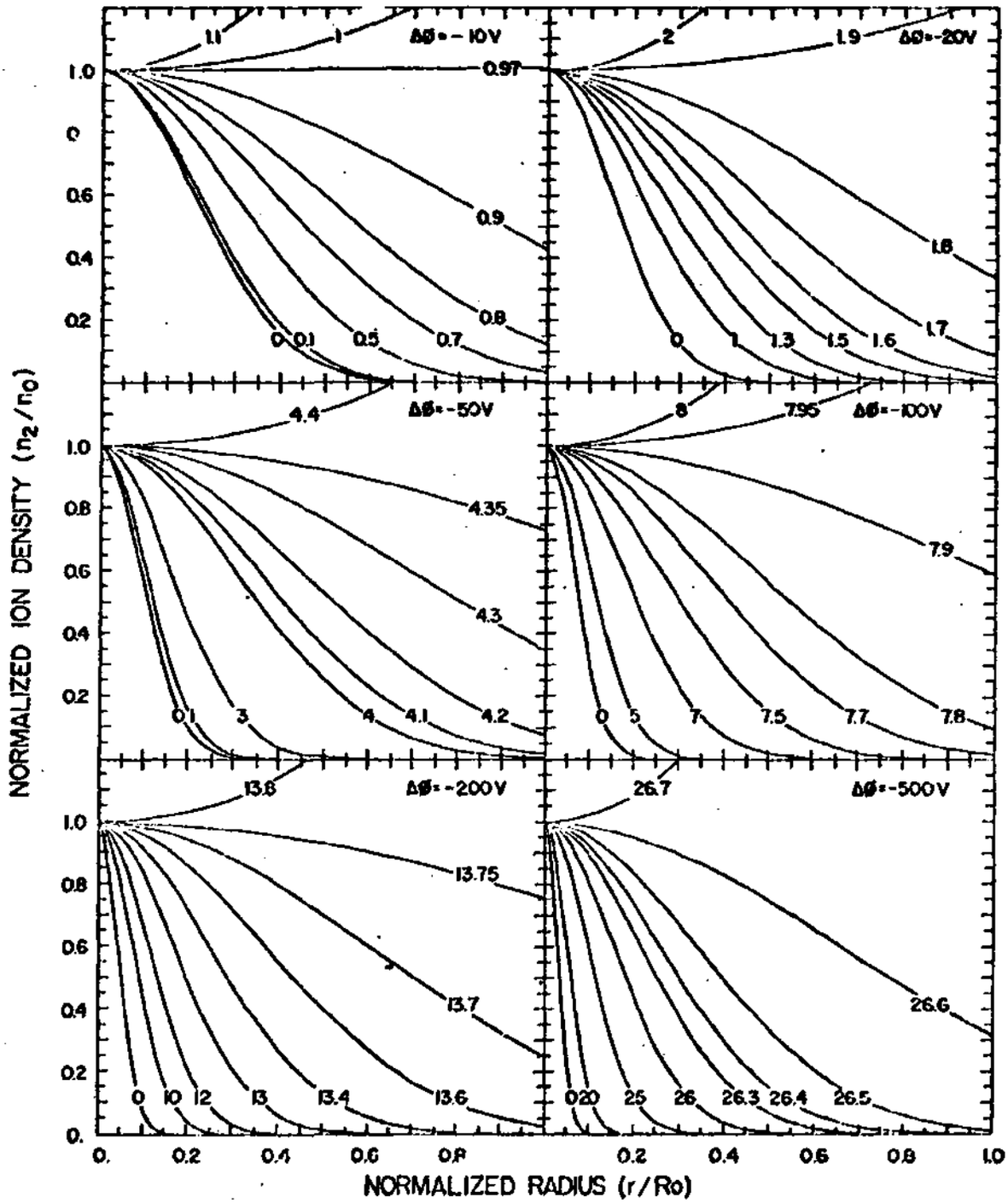

Fig. 2 - J.A. Bittencourt and G.O. Ludwig

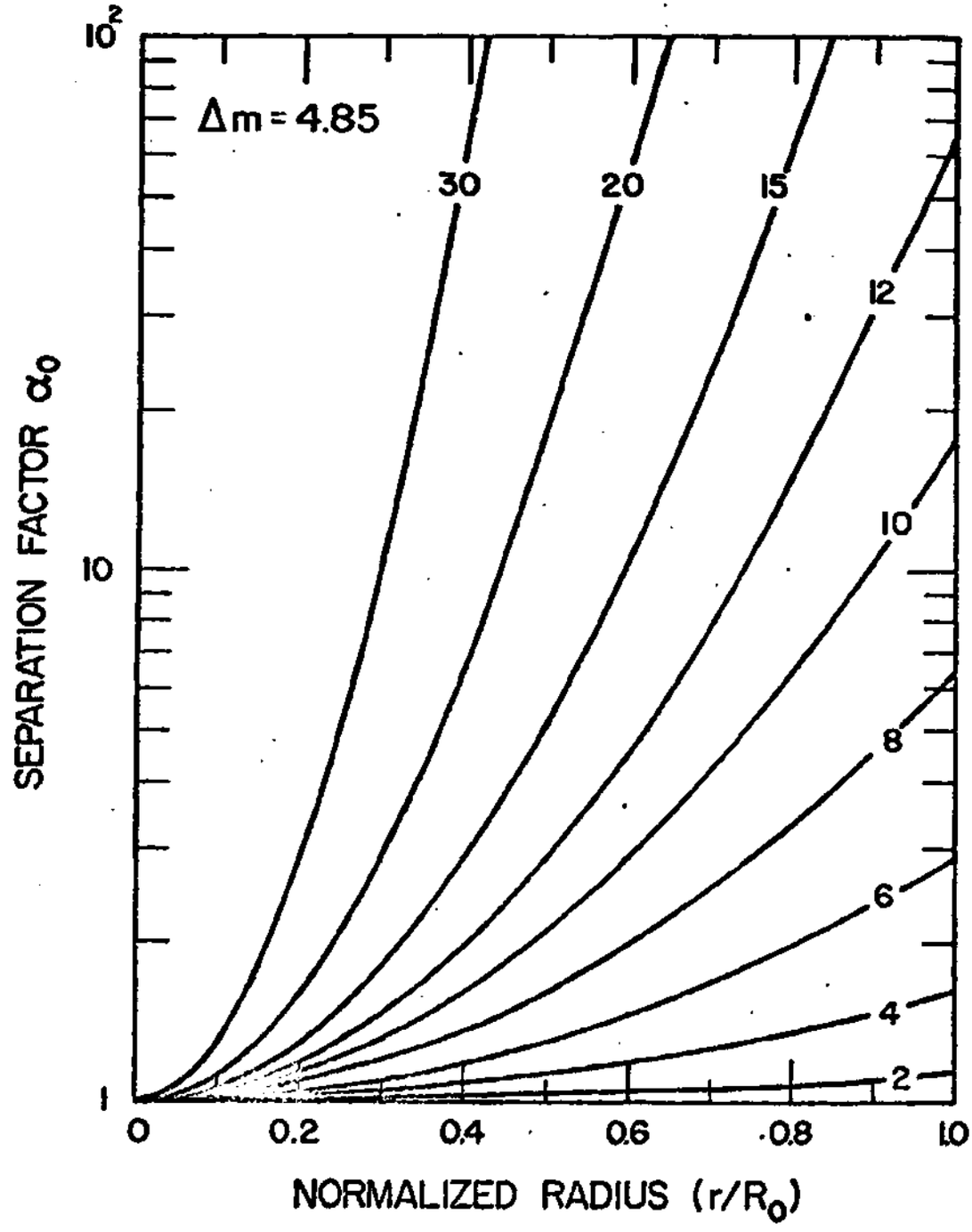

Fig. 3 - J.A. Bittencourt and G.O. Ludwig

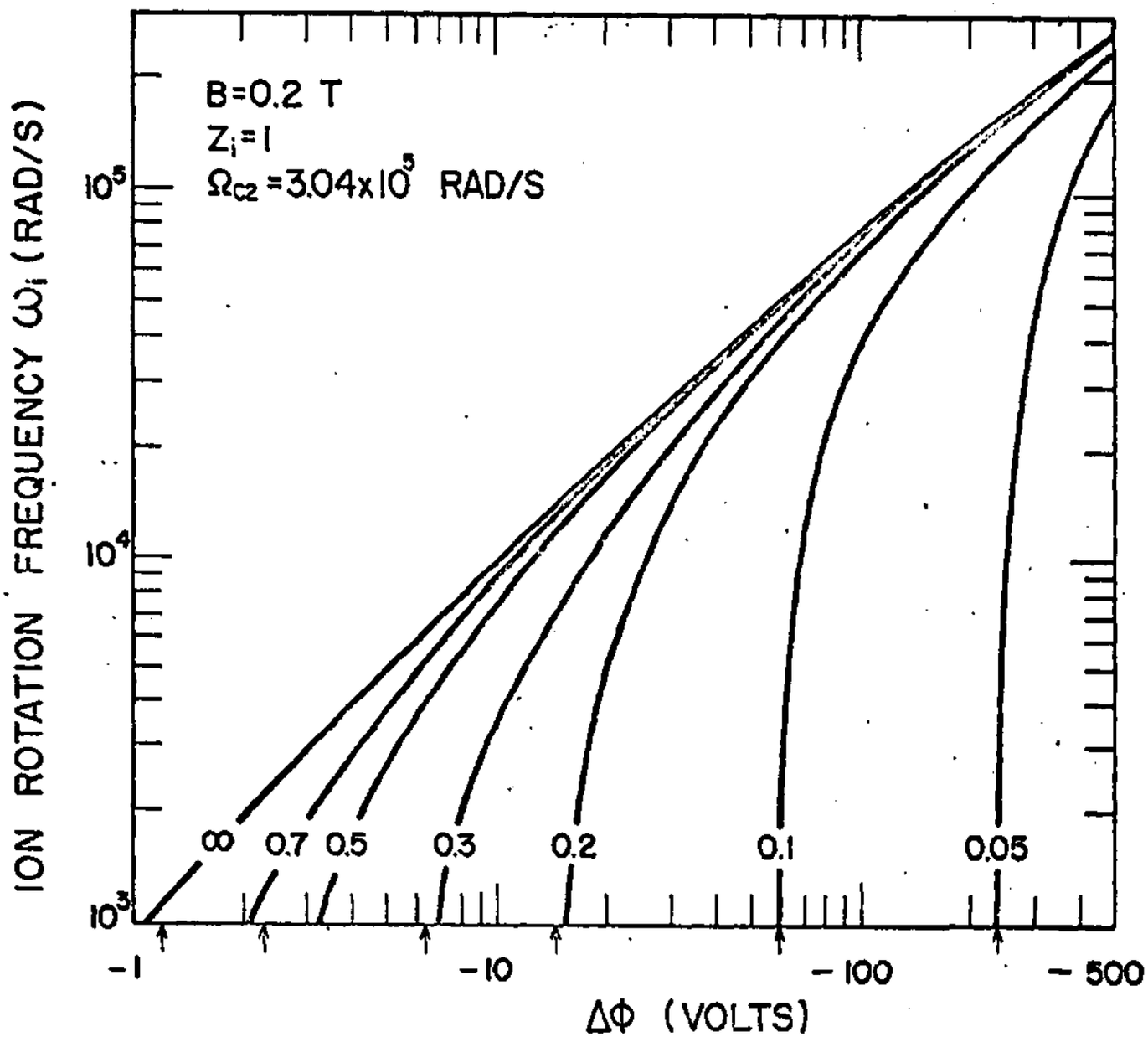

Fig. 4 - J.A. Bittencourt and G.O. Ludwig

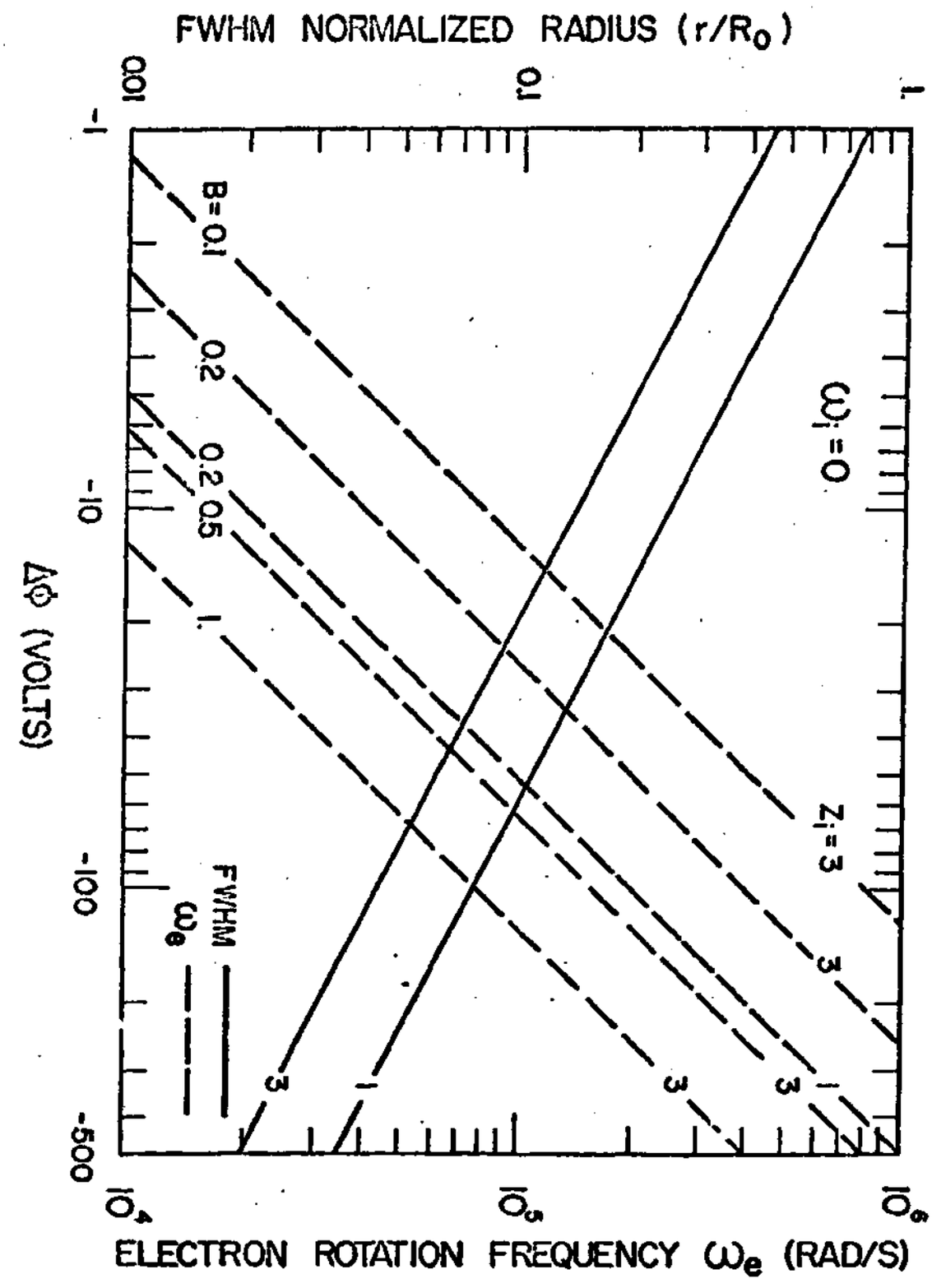

Fig. 5 - J.A. Bittencourt and G.O. Ludwig

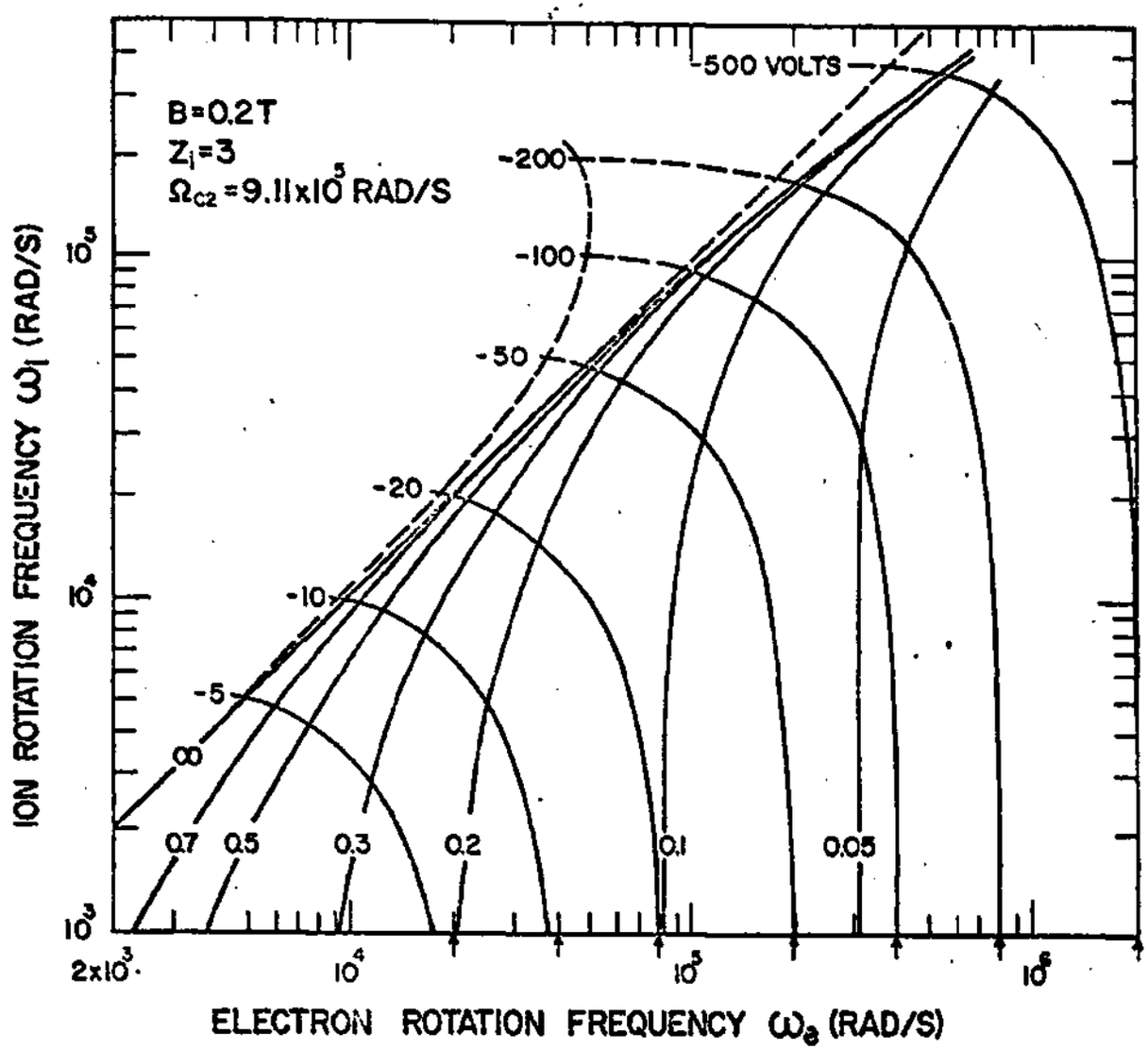

Fig. 6 - J.A. Bittencourt and G.O. Ludwig

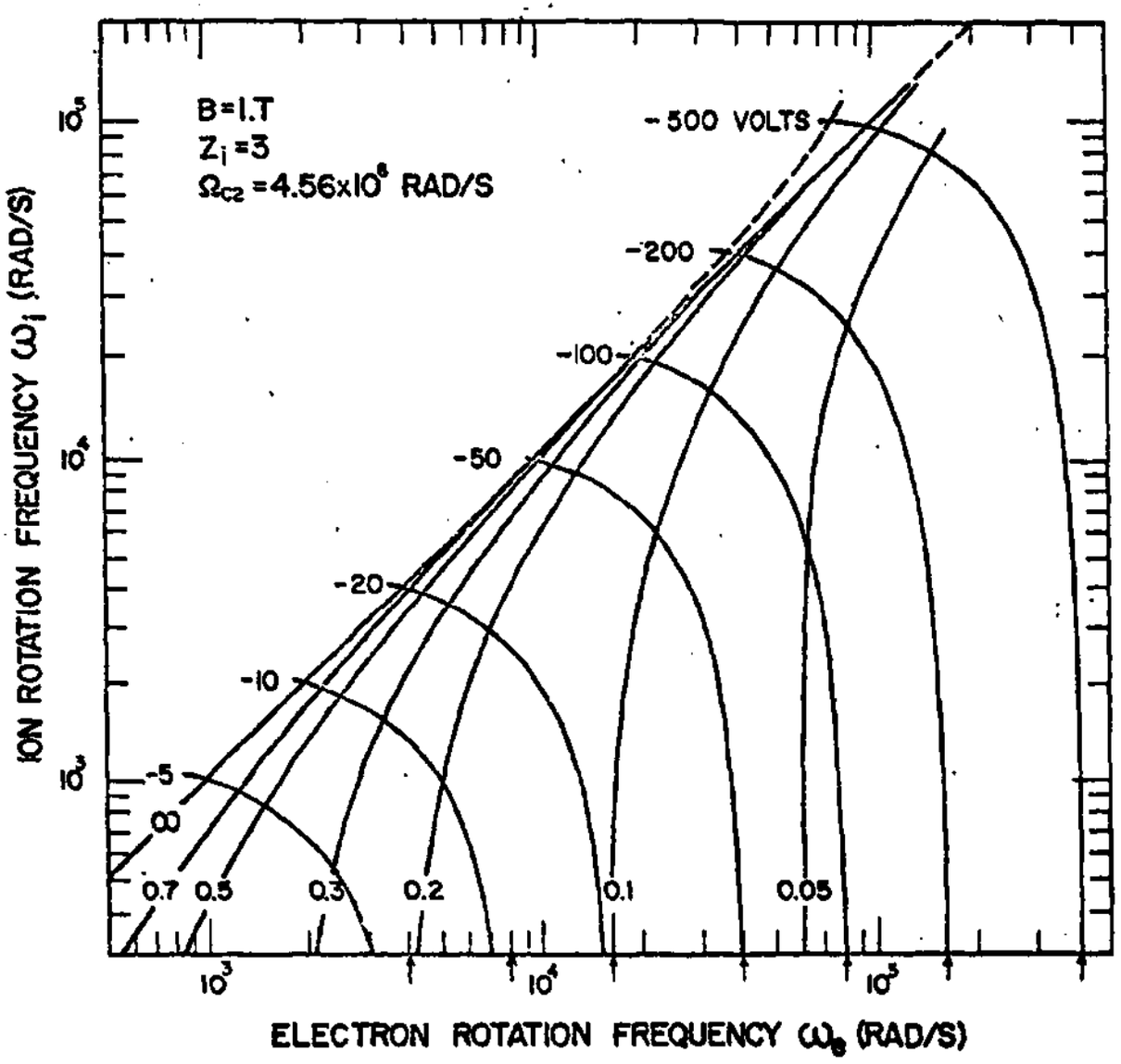

Fig. 7 - J.A. Bittencourt and G.O. Ludwig

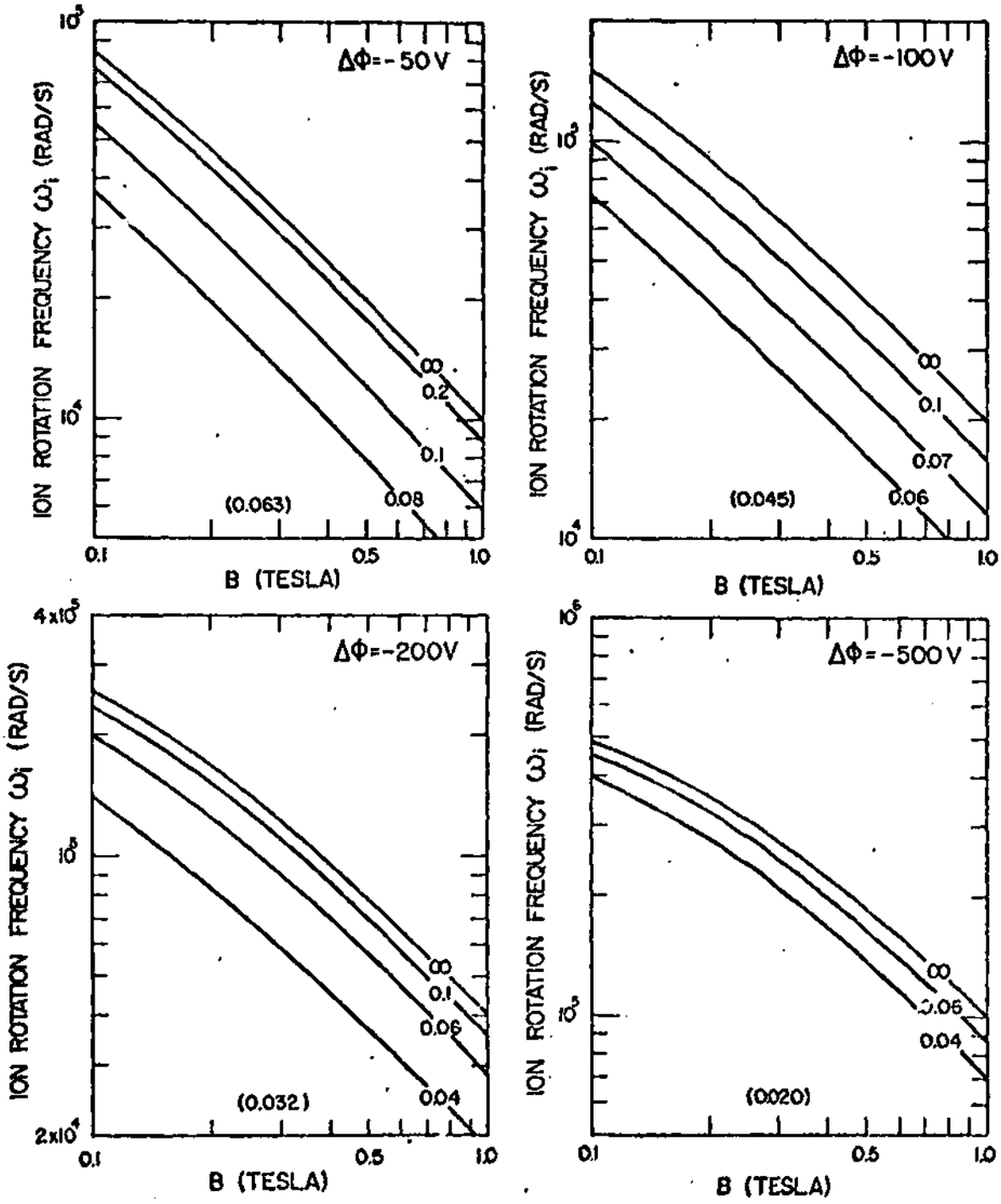

Fig. 8 - J.A. Bittencourt and G.O. Ludwig

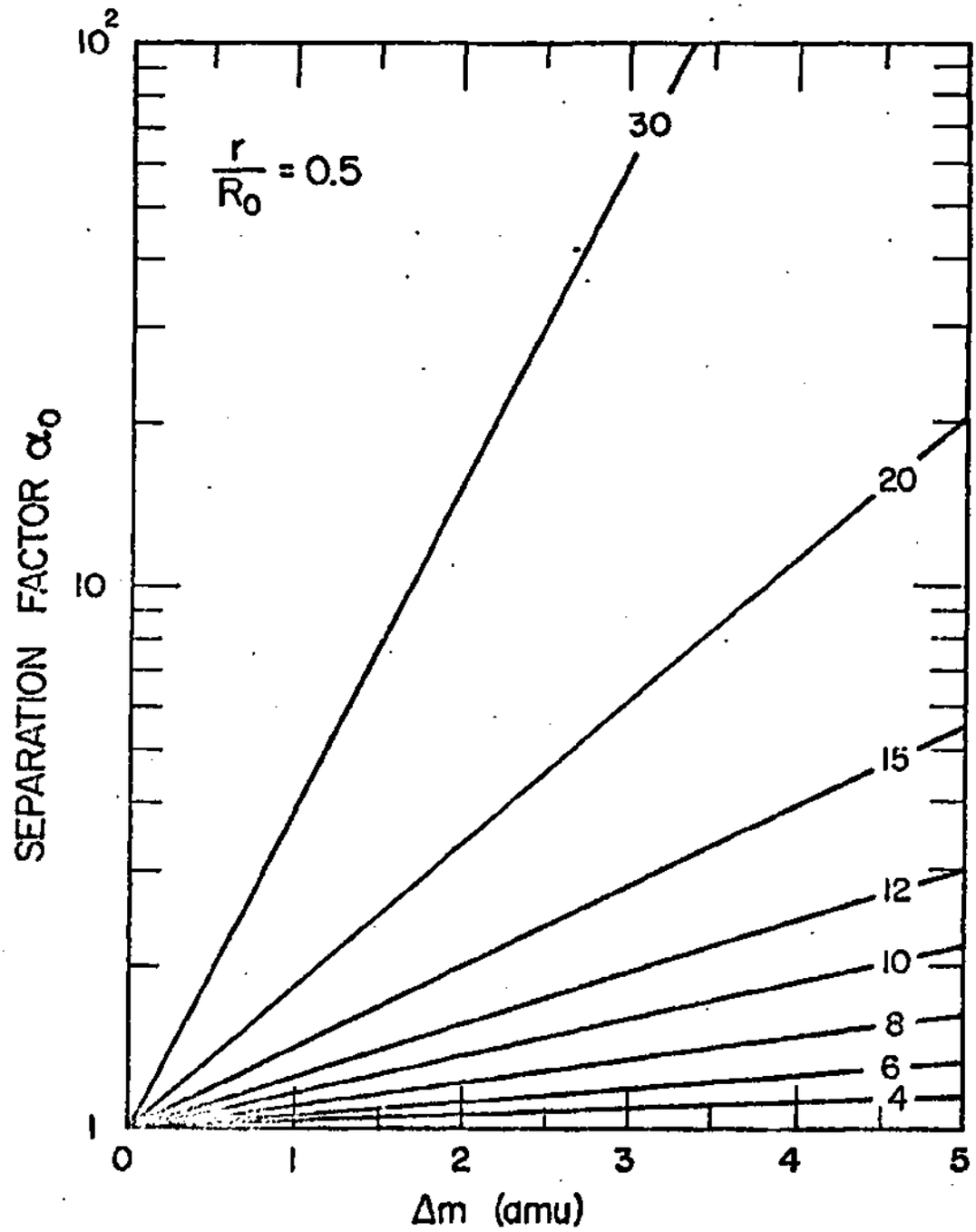

Fig. 9 - J.A. Bittencourt and G.O. Ludwig